CHAPTER 2

Solid State Synthesized $BiFeO_3$ Perovskite Based Fast Response White Light Photodetector*

Contents

*Part of this work has been published as:

Rishibrind Kumar Upadhyay et al., "Solid-State Synthesized $BiFeO_3$ Perovskite-Based Fast-Response White-Light Photodetector," ***IEEE Electron Device Letters,*** vol. 41, no. 8, pp. 1961-1964.

CHAPTER 2

Solid State Synthesized $BiFeO_3$ Perovskite Based Fast Response White Light Photodetector

2.1 Introduction

It has been discussed in chapter-1 that the inorganic perovskite Bismuth ferrite ($BiFeO_3$), also commonly referred to as BFO, has drawn considerable attention for photodetection applications [31], [81], [82], photovoltaic device [108], visible photodetector [83], sensitive switchable photodetector [109], multiferroic field-effect transistor [110], visible light photocatalytic activity [111], [112], memory storge [113], and self-powered photodetector with photovoltaic–pyroelectric coupled effect [84]. $BiFeO_3$ perovskite-based photodetector is fabricated in p-i-n diode structure with p-type and n-type oxides [29]. Mondal *et al.* [27] demonstrated a $BiFeO_3$ based efficient white light photodetector using indium doped tin oxide (ITO)/ZnO/BFO/ poly (3, 4-ethylenedioxythiophene): polystyrene sulfonate (PEDOT: PSS)/Au structure fabricated on the poly (ethylene terephthalate) (PET) substrate where ZnO and PEDOT: PSS were used for the electron transport layer (ETL) and hole transport layer (HTL), respectively. No other significant works are available on the BFO based white light photodetectors.

This chapter investigates the performance of an ITO/ZnO NPs/BFO NPs/ poly (3, 4-ethylenedioxythiophene): polystyrene sulfonate (PEDOT: PSS)/Ag structure-based white light photodetector fabricated on an ITO coated glass substrate using ZnO NPs (i.e. nanoparticles) for the ETL, BFO NPs for photoactive layer and PEDOT: PSS for HTL. The BFO NPs have been synthesized by solid-state route instead of commonly used solvothermal process and commonly used Au electrode metal has been replaced by low-

cost Ag in the structure considered by Mondal *et al.* [27]. A relatively thinner ZnO NPs layer than the BFO NPs layer is used to ensure the maximum absorption of the visible light in the $BiFeO_3$ (BFO) NPs layer. ZnO NPs is used for ETL while PEDOT: PSS is used for the HTL due to its excellent properties such as low-temperature processing, high transparency, conductivity and high optical transmittance in the range 300 nm to 800 nm [114]-[117]. The photoresponse characteristics of the proposed ITO/ZnO NPs/BFO NP_S/PEDOT: PSS/Ag structure has been measured using a monochromatic light over the wavelengths of 400-750 nm. The rise time and fall time are also measured. The outline of the present chapter is given below:

Section 2.2 presents the fabrication details of the proposed $BiFeO_3$ perovskite-based fast response white light photodetector. Various results and discussions related to the thin films and proposed photodetector are presented in section 2.3. Finally, section 2.4 has been used to conclude the objectives and outcomes of the research carried out in this chapter.

2.2 Experimental Details

In the present section, we have discussed the material synthesis, substrate cleaning, thin film deposition of ZnO NPs, inorganic perovskite $BiFeO_3$ NPs and PEDOT: PSS and device fabrication of an ITO/ZnO NPs/BFO NPs/PEDOT: PSS/Ag photodetector grown by the low-cost method.

2.2.1 Materials Synthesis

All the chemicals are used received from Sigma-Aldrich and Merck Chemicals without any further purifications. The ZnO NPs are synthesized by the sol-gel route. Zinc acetate dihydrate [Zn $(CH_3CO_2)_2 \cdot 2H_2O$] precursor is mixed with a solvent of an equal molar ratio of monoethanolamine (MEA) and 2-methoxy ethanol in ambient condition.

Initially, 1 M (2.1949 gm) zinc acetate [Zn $(CH_3CO_2)_2 \cdot 2H_2O$] is dissolved in 2-methoxy ethanol (10 ml) and stirred the solution continuously for more than 2 hours on a hot plate to gradually increase its temperature up to a fixed temperature of 60°C. MEA (reagent) (1.2 ml) is then quickly injected into the stirred solution at 60°C for growing colloidal ZnO NPs [118]. A schematic representation of the synthesis of ZnO NPs is shown in Figure 2.1.

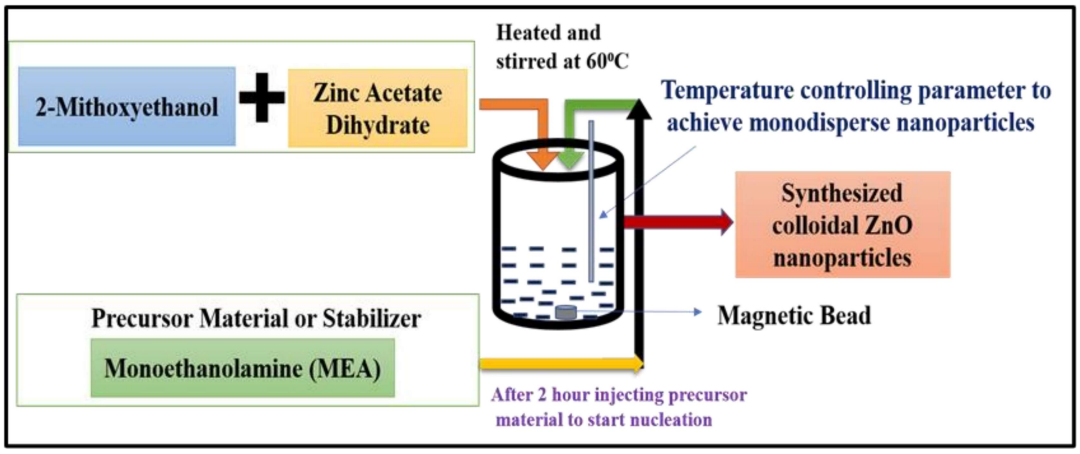

Figure 2.1: Synthesis of the ZnO nanoparticles.

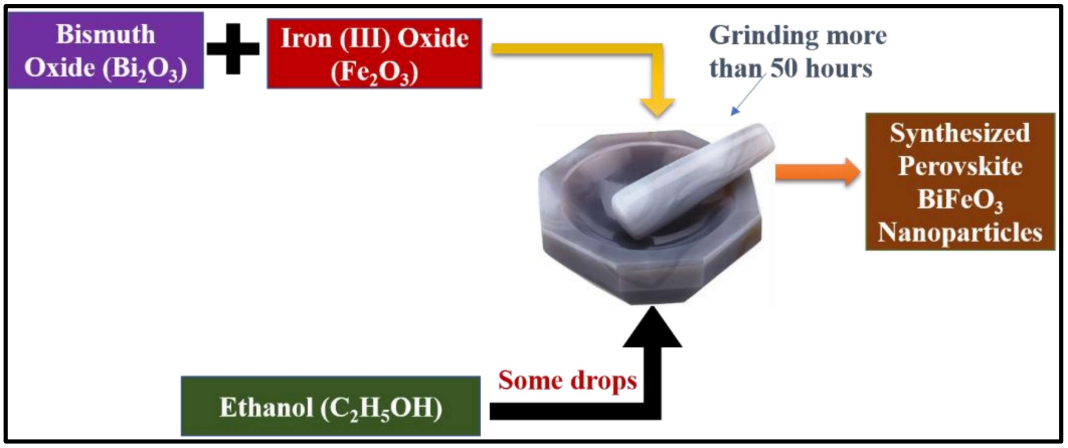

Figure 2.2: Synthesis of the perovskite $BiFeO_3$ nanoparticles.

The $BiFeO_3$ NPs are synthesized by the solid-state route using a mortar and pestle grinding by hand for more than 50 hours. In this process, the 3.72375 gm of bismuth oxide (Bi_2O_3) and (1.2762 gm) iron (III) oxide (Fe_2O_3) are first mixed in a stoichiometric ratio. A few drops of ethanol is added to it for better mixing [41]. Finally, the calcinated BFO NPs are obtained by drying the resultant mixture in two steps: first at 600°C for 1 hour

and then at 800°C for 2 hours [42]. A schematic representation of the synthesis of the perovskite $BiFeO_3$ NPs is shown in Figure 2.2.

2.2.2 Device Fabrication

In this section, we are discussing the substrate cleaning process, thin-film deposition in detail.

2.2.2.1 Substrate Cleaning

In the present work indium doped tin oxide (ITO) coated glass substrates with thickness ~1.1 mm and resistivity ~15-20 (ohm.cm) was cut into small regular square-shaped (15×15 mm^2) using a diamond cutter. The small ITO glass substrate piece was cleaned thoroughly, at first, ITO coated glass substrates were sequentially cleaned in an ultrasonic cleaning bath in a 5% soap solution to remove dust particles for 15 min., then deionized (DI) water with a resistivity of ~18 (MΩ.cm) to get rid of chemical residues for 15 min., then acetone (C_3H_6O) to remove the organic remnants/contaminants from the substrate for 15 min., at last, cleaned by isopropanol (C_3H_8O) for 10 minutes to remove organic residues left on substrate. Then, the substrates were treated by plasma cleaning in the presence of oxygen and argon for 15 minutes to increase the hydrophilicity of ITO coated glass substrate.

2.2.2.2 Thin Film Deposition

In the first deposition step, ZnO NPs dispersed solution was deposited on the as cleaned ITO coated glass substrate by the spin coating unit (TSE, Model SPM-150LC, Germany) at 2000 rpm for 30 s. The process was optimized and repeated two times (at same speed and duration) to obtain a ZnO NPs layer thickness of ~100 nm. ZnO NPs coated ITO samples were then annealed at 450^0C for 2 hours in a muffle furnace. In the second step, the BFO ($BiFeO_3$) NPs were first mixed in methanol to obtain a uniformly

dispersed BFO NPs solution. This solution was then used to grow a thin layer of BFO NPs on the ZnO NPs layer using the spin coating method at 1500 rpm for 40 s to obtain a $BiFeO_3$ NPs layer of ~200 nm thickness and this deposition process was repeated one more time. The film BFO NPs deposited on the ZnO NPs coated ITO coated samples were then annealed at 300°C for 1 hour in an ambient air environment. In the third step, a solution of PEDOT: PSS was deposited on the BFO NPs film at 2000 rpm for 40 s. For contact electrode formation, Ag (99.99%) metal dots of ~2 mm diameter (device area 0.0314 cm^2) and ~100 nm thickness were fabricated on the PEDOT: PSS film by thermal evaporation unit (Model No. FL400, SMART COAT 3.0 A, Hind High Vacuum India) with the shadow mask technique. The vacuum level was maintained in the range of 10^{-6} mbar with a deposition rate of 0.02 Å/s in the thermal evaporation unit. The thicknesses of different layers of the device were measured using the optical spectrometer commonly known as F20-UV, thin-film analyzer (Model No. SDT2, Filmetrics USA) instrument.

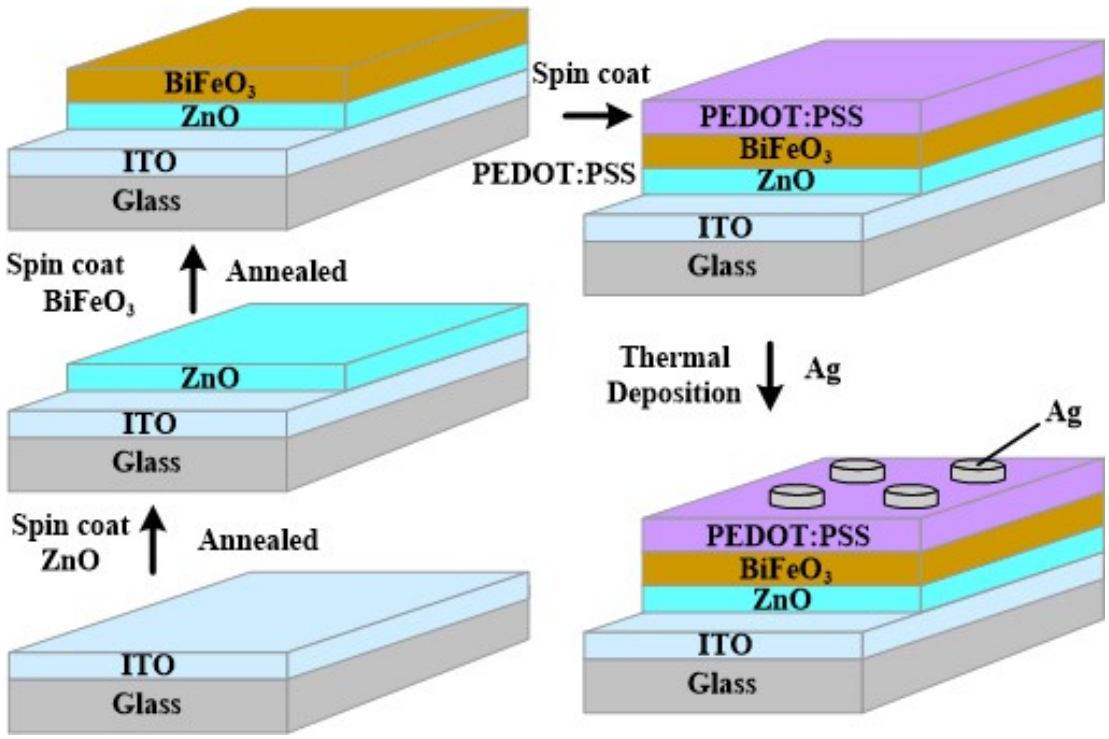

Figure 2.3: Schematic representation of the fabricated steps used for fabrication of $BiFeO_3$ based white light photodetector device.

A schematic representation of the fabricated steps used for the fabrication of $BiFeO_3$ based white light photodetector is shown in Figure 2.3.

2.3 Results and Discussion

In this section, structural, optical, and electrical characterization of $BiFeO_3$ perovskite thin film-based device, are presented.

2.3.1 Thin Film Characterizations

(a) Crystallographic orientation by XRD Analysis

The crystalline structure of ZnO nanoparticles and $BiFeO_3$ nanoparticles have been investigated by X-ray diffraction (RIGAKU-Smart XDMAX, PC-20, 18-Kw Cu rotating anode, Rigaku, Tokyo) at room temperature.

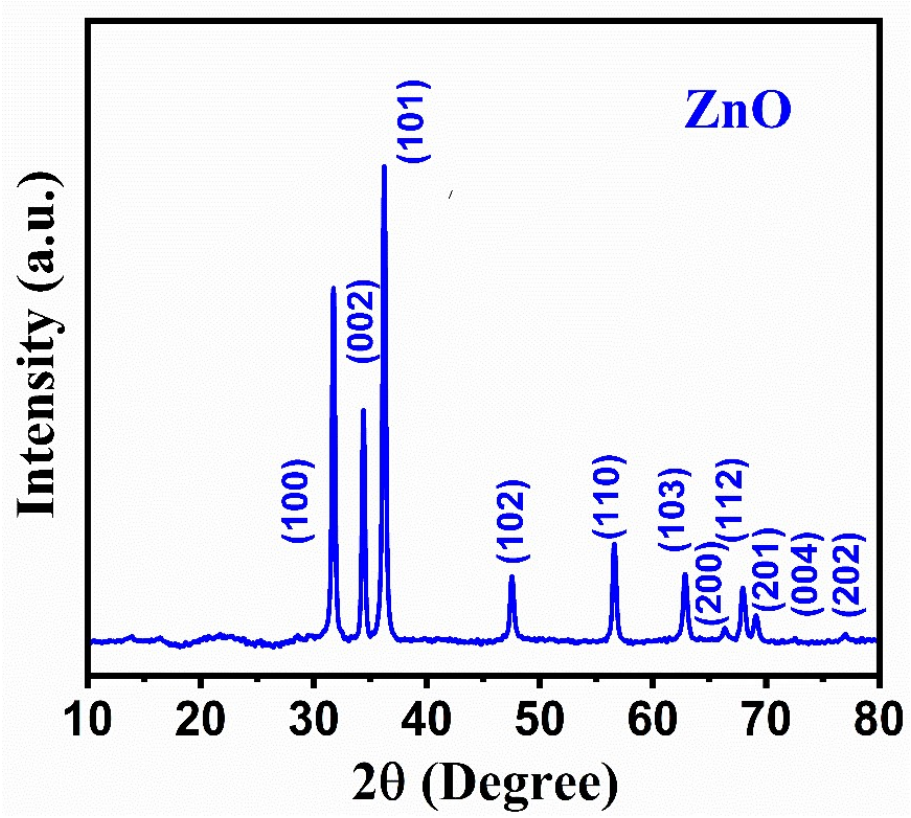

Figure 2.4: XRD peaks of the ZnO NPs thin film coated on the glass substrate using X-ray diffraction (RIGAKU-Smart XDMAX, PC-20, 18-Kw Cu rotating anode, Rigaku, Tokyo) at room temperature.

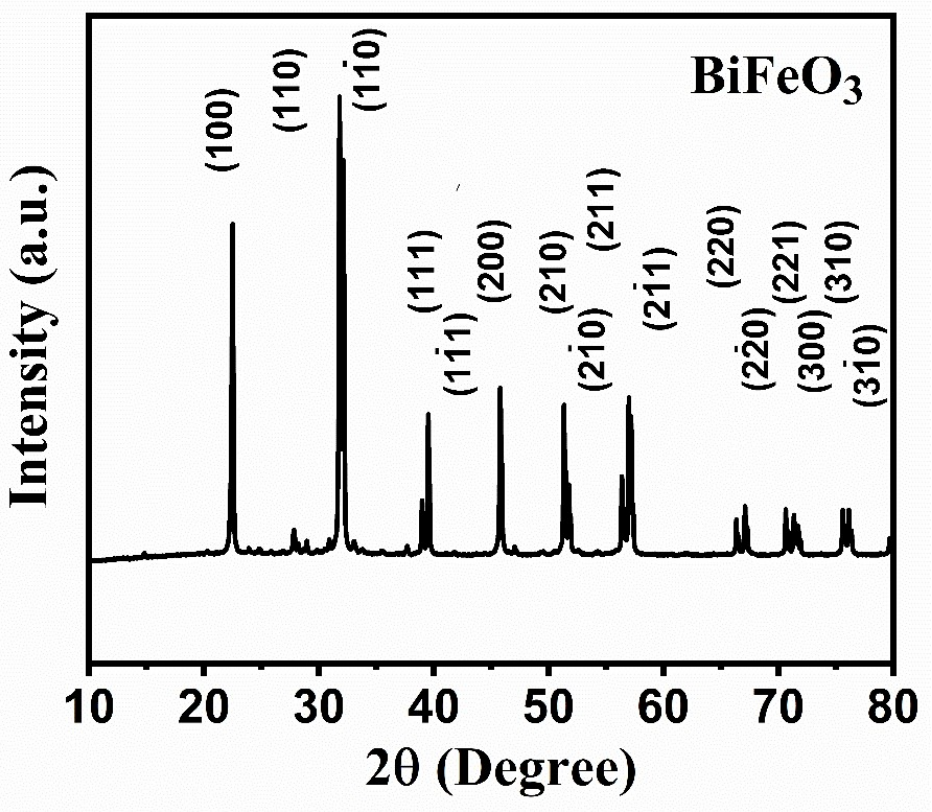

Figure 2.5: XRD peaks of the $BiFeO_3$ nanoparticles coated on the glass substrate using X-ray diffraction (RIGAKU-Smart XDMAX, PC-20, 18-Kw Cu rotating anode, Rigaku, Tokyo) at room temperature.

The obtained XRD spectra of ZnO NPs has been shown in Figure 2.4. The diffraction peaks found in the XRD spectra of ZnO NPs at 31.2°, 33.9°, 35.8°, 47.1° and 56.1° are assigned to the diffractions from the (100), (002), (101), (102) and (110) planes, respectively. The obtained diffraction peaks are well matched to the hexagonal wurtzite structure of ZnO (JCPDS card No. 36-1451, a = 0.325 nm and c =0.521 nm) without any contaminations and high purity [119], [120].

While major diffraction peaks observed in XRD spectra of $BiFeO_3$ NPs samples at 22.48°, 31.8°, 39.52°, 47.04°, 51.34°, 57.00° are assigned to (100), (110), (111), (200), (210) and (211) planes, respectively. The obtained diffraction peaks are well matched to the rhombohedral structure of $BiFeO_3$ [42], [121]. The obtained XRD spectra of $BiFeO_3$ NPs has been shown in Figure 2.5.

(b) Surface Morphology

The surface morphology of the synthesized ZnO NPs and perovskite $BiFeO_3$ NPs is investigated using a high-resolution scanning electron microscope (HRSEM, Nova Nano SEM 450, USA) at room temperature. The HRSEM image of the ZnO NPs based thin film annealed at 450ºC for 2 hours is shown in Figure 2.6. It's clear from the HRSEM image that the ZnO nanoparticles deposited on the glass substrate have high density and uniformity with average particles size in the range of 50-80 nm. The HRSEM image of the perovskite $BiFeO_3$ (BFO) thin film annealed at 300ºC for 1 hour is shown in Figure 2.7. It's clear from the HRSEM image of $BiFeO_3$ thin film that the nanoparticles of $BiFeO_3$ have uniformly grown in high density with average particles of 100-150 nm (larger particles comparable to ZnO NPs) .

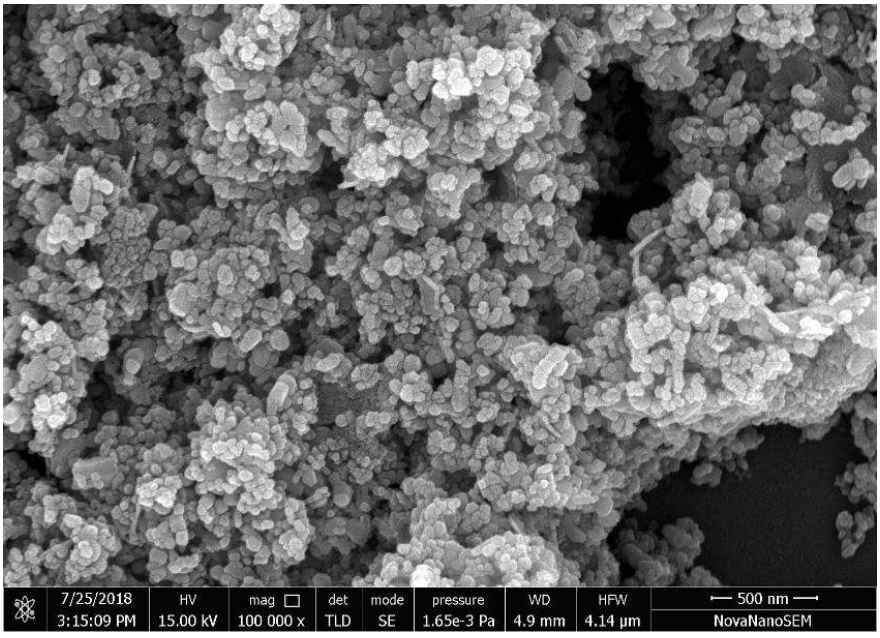

Figure 2.6: HRSEM image of the ZnO nanoparticles on the glass substrate using high-resolution scanning electron microscope (HRSEM, Nova Nano SEM 450, USA).

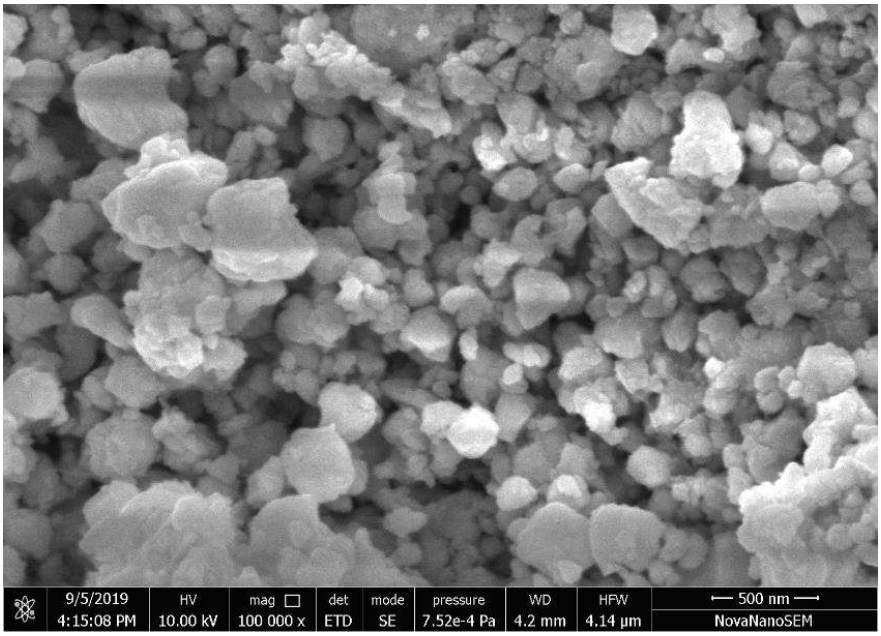

Figure 2.7: HRSEM image of the $BiFeO_3$ nanoparticles on the glass substrate using high-resolution scanning electron microscope (HRSEM, Nova Nano SEM 450, USA).

(c) UV-Vis Analysis

Ultraviolet-Visible (UV-Vis) spectroscopy (V-770 from JASCO, Japan) provides information of absorption or reflectance spectra which is typically used for bandgap estimation and optical absorbance of materials. According to Beer Lambert's equation, absorption coefficient α of sample material is given by following relation [122]:

$$\alpha = 2.303 Abs \frac{(\lambda)}{t} \qquad \text{.....(2.1)}$$

where t is the thickness of thin film and absorbance coefficient Abs (λ) of the thin film is measured from the absorbance curve, experimentally measured by UV-visible (UV-vis) spectroscopy. At room temperature, the measured Abs (λ) of ZnO nanoparticles and perovskites $BiFeO_3$ thin film on glass substrate are shown in Figure 2.8. For ZnO NPs thin film, we obtained the maximum absorption in the UV region, with a strong peak corresponding to 370 nm wavelength, while in the case of $BiFeO_3$ thin film, we obtained maximum absorption in the visible region making this heterostructure suitable as a white light photodetector.

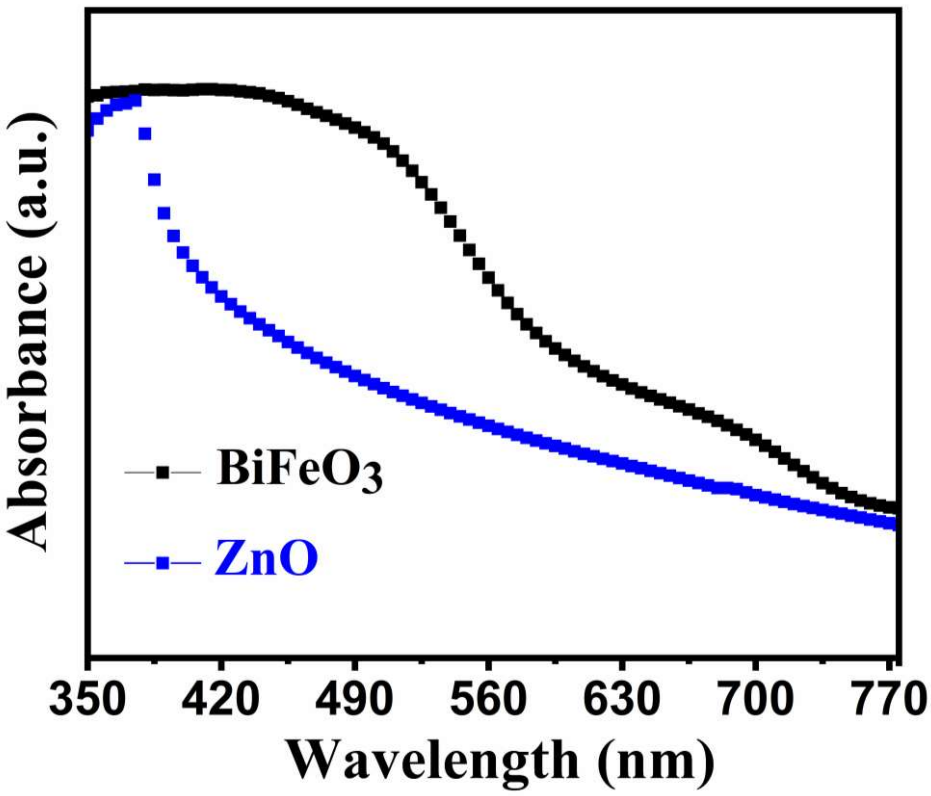

Figure 2.8: Absorbance spectra of the perovskite $BiFeO_3$ thin film and ZnO nanoparticles thin film coated on the glass substrate using (UV-Vis) spectroscopy (V-770 from JASCO, Japan).

Further, the absorption coefficient as a function of the energy of a photon is expressed by Tauc relation [50], [122]:

$$(\alpha h\nu)^{1/n} = \beta(h\nu - E_g) \qquad \text{.....(2.2)}$$

where β, α, h, ν, Eg and n are the constants representing the band tailing parameter, absorption coefficients, Plank constant, light frequency, optical band gap, and empirical constant, respectively. The value of n depends on material properties, which are taken as 1/2, 2, 3/2, and 3 for direct allowed, indirect allowed, direct forbidden, and indirect forbidden transitions, respectively.

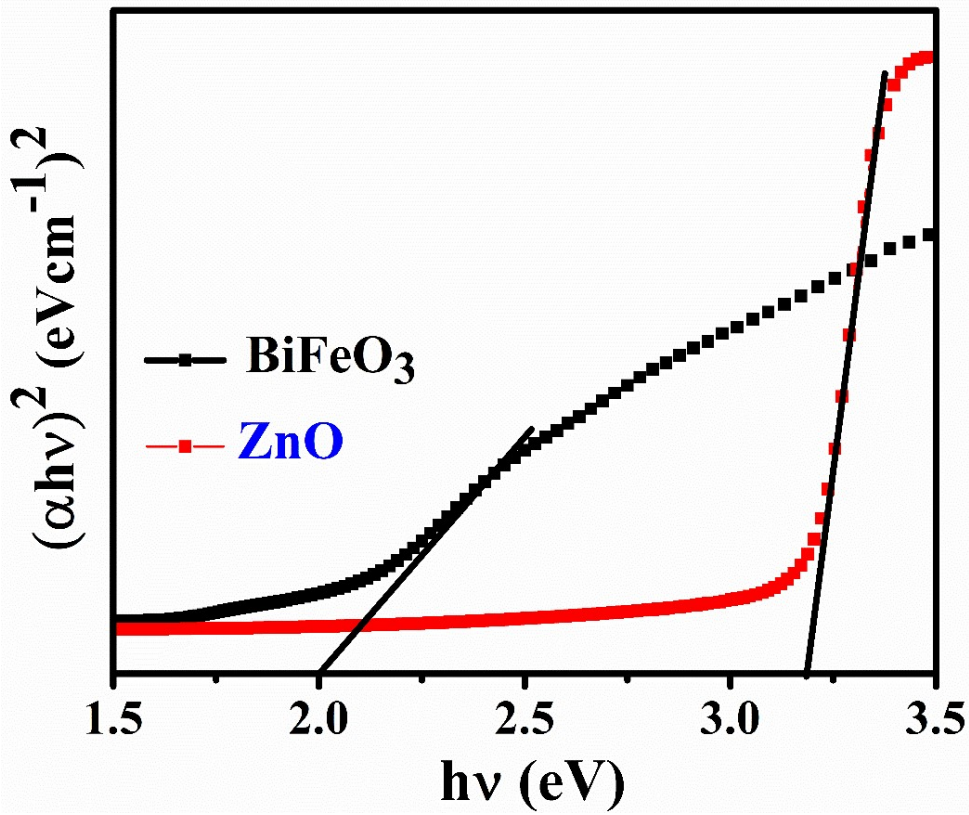

Figure 2.9: Tauc plot of the perovskite $BiFeO_3$ thin film and ZnO nanoparticles thin film coated on the glass substrate for bandgap calculation using (UV-Vis) spectroscopy (V-770 from JASCO, Japan).

Hence by extrapolating the linear part of $(\alpha h\nu)^{1/n} = \beta(h\nu - E_g) = 0$ (as displayed in Figure 2.9) the estimated optical band gaps of ~2.0 eV and ~3.2 eV is found for $BiFeO_3$ thin film and ZnO nanoparticles thin film, respectively.

2.3.2 Electrical Characterizations

After investigating the thin film properties, we now examined the room temperature electrical characterization via capacitance-voltage (*C-V*) characteristics and current-voltage *(I–V)* characteristics measurements for the fabricated device.

(a) capacitance-voltage (C-V) characteristics

The room temperature (T ~303 K) capacitance-voltage (*C-V*) characteristics are performed at 1000 Hz frequency using a semiconductor parameter analyzer (B1500A from Keysight, USA) for ITO/ZnO NPs/BFO NPs/PEDOT: PSS/Ag device. The *C-V*

measurement has been performed to include only the depletion layer capacitance by avoiding the excess capacitance due to interface states at low frequencies [50], [123]. Capacitance-voltage *C-V* characteristics of the fabricated heterostructure device is shown in Figure 2.10. The existence of capacitance confirms the formation of a depletion region at the junction of the heterojunction device. Negative capacitance due to the different series resistance and interface states at different frequencies [124], [125].

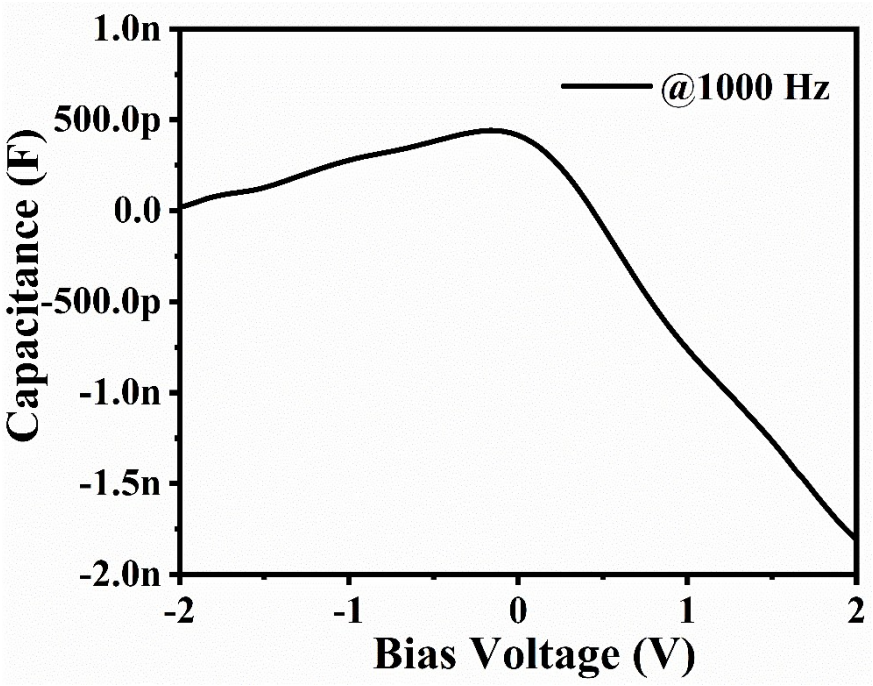

Figure 2.10: Capacitance voltage *(C-V)* characteristics of the fabricated heterostructure device at 1000 Hz frequency using a semiconductor parameter analyzer (B1500A from Keysight, USA).

(b) Energy Band Diagram

Now we discussed the photodetection mechanism for the fabricated photodetector device. Note that the operation of the ITO/ZnO NPs/BFO NPs/PEDOT: PSS/Ag heterojunction device under white light illumination involves three steps:

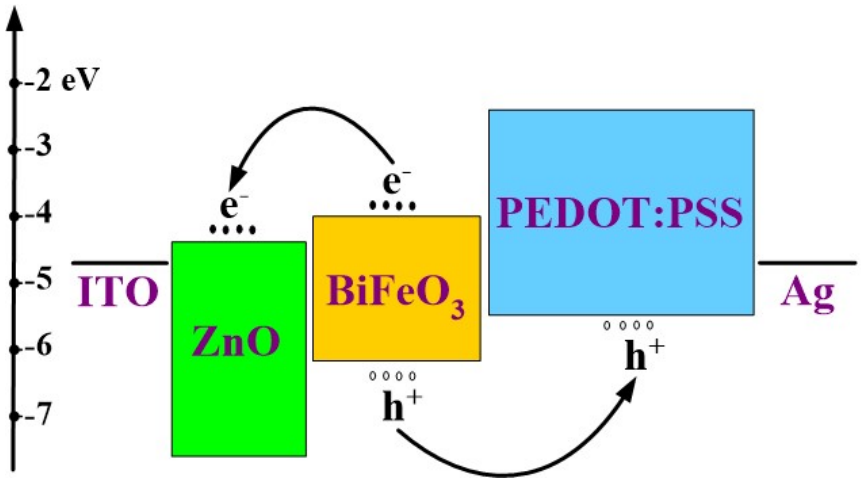

Figure 2.11: Schematic energy band diagram of the proposed heterojunction photodetector.

(i) The generation of charge carrier by incident light.

(ii) The separation and transport of charge carrier by internal field in the depletion region.

(iii) Extraction of charge carrier as terminal current to provide output signal [50], [126].

The operation of the ITO/ZnO NPs/BFO NPs/PEDOT: PSS/Ag heterojunction photodetector has been demonstrated in Figure 2.11 through an energy band diagram of the fabricated device under light illumination and in reverse bias condition. The proposed photodetector device is illuminated from (Glass/ITO Side) to gain 100% illumination area. Note that the major portion of the light will be reflected back to open space from the metal surface if the device is illuminated from the metal contact side. The ZnO NPs layer is used as an electron transport layer (ETL) while PEDOT: PSS layer is used as a hole transport layer (HTL) in the proposed device. The photo-generated electron moves towards the ZnO NPs layer while the hole moves towards the metal (Ag) electrode. The excess photogenerated electron-hole pairs (EHPs) in the active region (i.e. depletion region of $BiFeO_3$) are drifted out to the inherent electric field of the depletion region.

(c) current-voltage (I–V) characteristics

The measured current-voltage *(I–V)* characteristics of the ITO/ZnO NPs/BFO

NPs/PEDOT: PSS/Ag heterojunction have been shown in Figure 2.12. The current-voltage *(I–V)* characteristics are measured at room temperature and in -2 V to 2 V bias voltage range by using a semiconductor parameter analyzer (B1500A from Keysight, USA) under dark and light illumination of 1 sun (obtained from solar simulator manufactured by PET, USA) condition. The dark current and photocurrent of 0.0468 µA and 0.685 µA are found under the forward bias of 2 V while 0.297 µA and 2.84 µA under the reverse bias of 2 V, respectively. For reverse saturation current calculation, we compare the current-voltage *(ln I–V)* characteristics as shown in Figure 2.13, of the fabricated white light photodetector. A reverse saturation current of ~8.8×10^{-11}A is calculated from the standard diode equation in the dark condition [50].

$$I = I_0 \left\{ exp\left(qV/\eta kT\right) - 1 \right\} \qquad \text{..... (2.3)}$$

where q is the electronic charge, η is the ideality factor of the heterojunction, V is the bias voltage, I_0 is the reverse saturation current, and T is the absolute temperature.

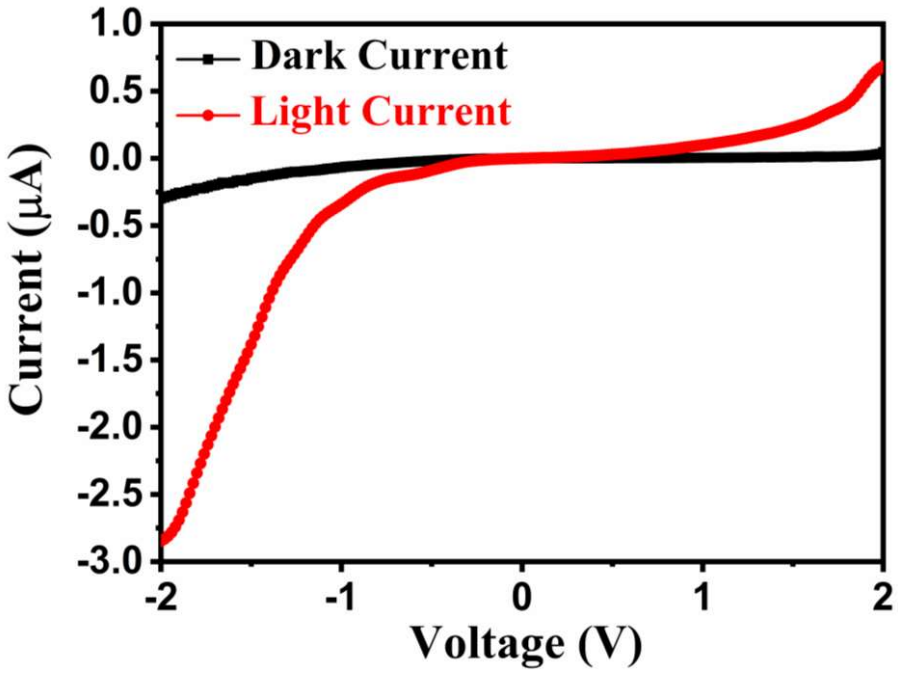

Figure 2.12: Current-voltage (*I-V*) characteristics of the proposed heterojunction photodetector using a semiconductor parameter analyzer (B1500A from Keysight, USA) under dark and light illumination of 1 sun (obtained from solar simulator manufactured by PET, USA) condition.

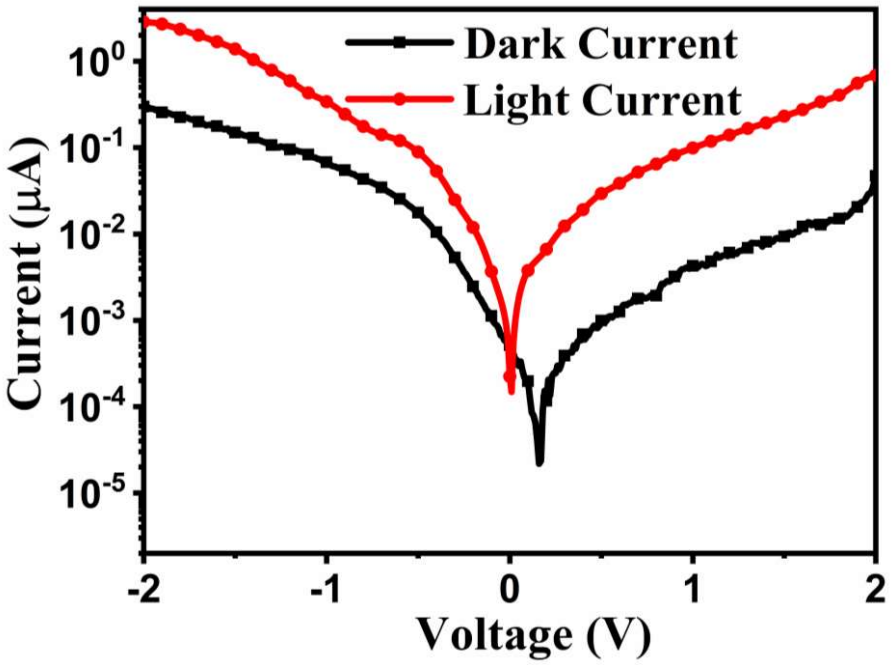

Figure 2.13: Logarithmic current-voltage (*ln I-V*) characteristics of the proposed heterojunction photodetector using a semiconductor parameter analyzer (B1500A from Keysight, USA) under dark and light illumination of 1 sun (obtained from solar simulator manufactured by PET, USA) condition.

2.3.3 Optical Characterizations

The wavelength (λ) dependent optical power density P_{opt} (λ) of the incident monochromatic light is measured by a power meter (PM100D, Thorlabs). Figure 2.14 shows the responsivity (R) of the proposed photodetector measured over 400 to 750 nm obtained from a monochromator (SP2150i from Princeton Instruments, USA) along with a halogen light source. The responsivity of the proposed photodetector is calculated using the following relation:

$$R(\lambda) = I(\lambda, V) / AP_{opt}(\lambda) \quad \text{..... (2.4)}$$

where I (λ, V) = (I_{light} - I_{dark}) is the photocurrent of the photodetector. I_{light} and I_{dark} denote the current under the illuminated condition and dark condition, respectively. A is the exposed effective area of the photodetector for irradiation and P_{opt} (λ) expresses the density of incident optical power. The maximum value of responsivity ~34 mA W^{-1} for the proposed photodetector is obtained over the specified visible range of 450-650 nm at

an applied bias voltage of -2V.

With the help of the responsivity of the proposed photodetector we can easily calculate the external quantum efficiency (EQE) of the proposed photodetector by using the following relation:

$$EQE(\%) = 1240 \frac{R(\lambda)}{\lambda} * 100 \quad \text{..... (2.5)}$$

The maximum value of ~8.8% external quantum efficiency (EQE) of the proposed photodetector is obtained over the specified visible range of 450-650 nm at an applied bias voltage of -2V. Figure 2.15 shows the external quantum efficiency (EQE) of the proposed photodetector measured over 400 to 750 nm.

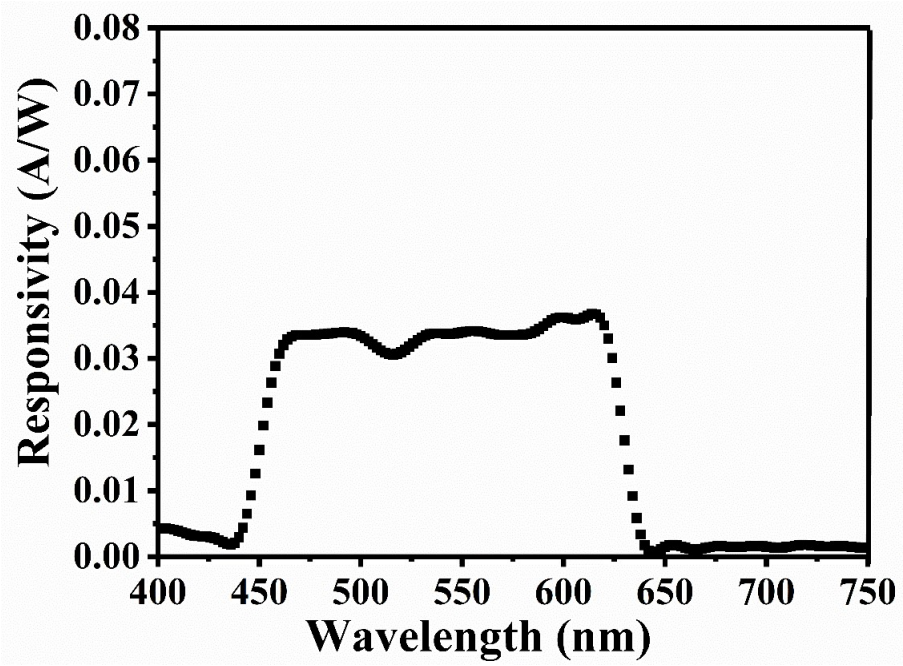

Figure 2.14: Responsivity of the proposed photodetector device against wavelength in the range of 400-750 nm at an applied bias voltage of -2V using a monochromator (SP2150i from Princeton Instruments, USA) along with a halogen light source.

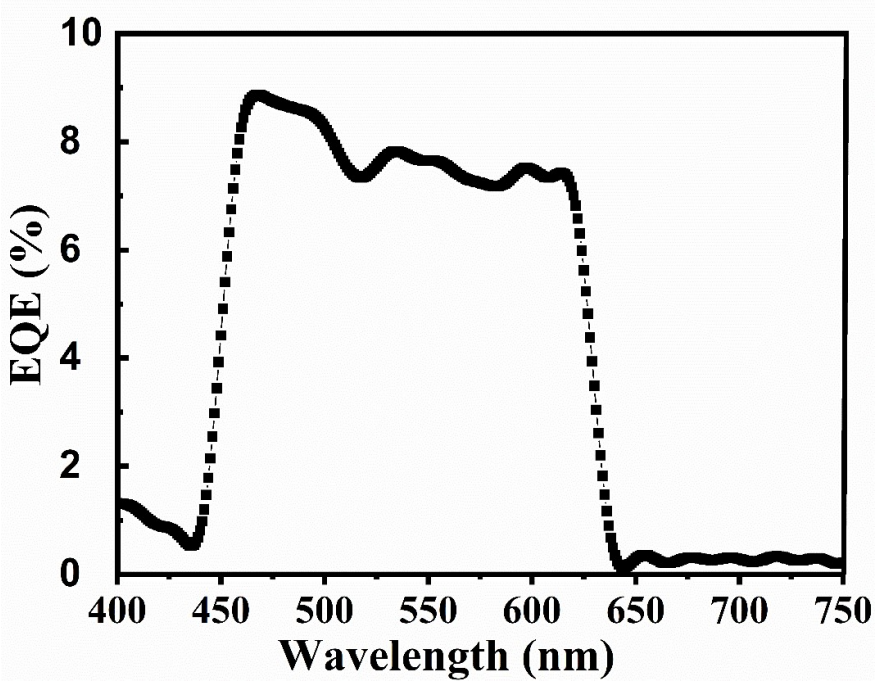

Figure 2.15: External quantum efficiency (EQE) of the proposed photodetector device against wavelength in the range of 400-750 nm using a monochromator (SP2150i from Princeton Instruments, USA) along with a halogen light source.

Further, the repeatability of the results and photoresponse speed of the photodetector are investigated using transient response measurement. For repeatability of the results, we have used a digital multimeter (Agilent, 34410 A) and LED source with an on-off time of 20 s each. The ON-OFF pulsating is obtained by using an Arduino™ microcontroller and the digital multimeter is controlled by Lab View™. The LED source has a white light wavelength with an optical power density of ~40.3 $\mu W/cm^2$ measured by using a power meter (PM100D, Thorlabs). The obtained results (at ambient room temperature (27°C) and biased voltage of -2V) are plotted between times (in sec.) and current (μA) as shown in Figure 2.16.

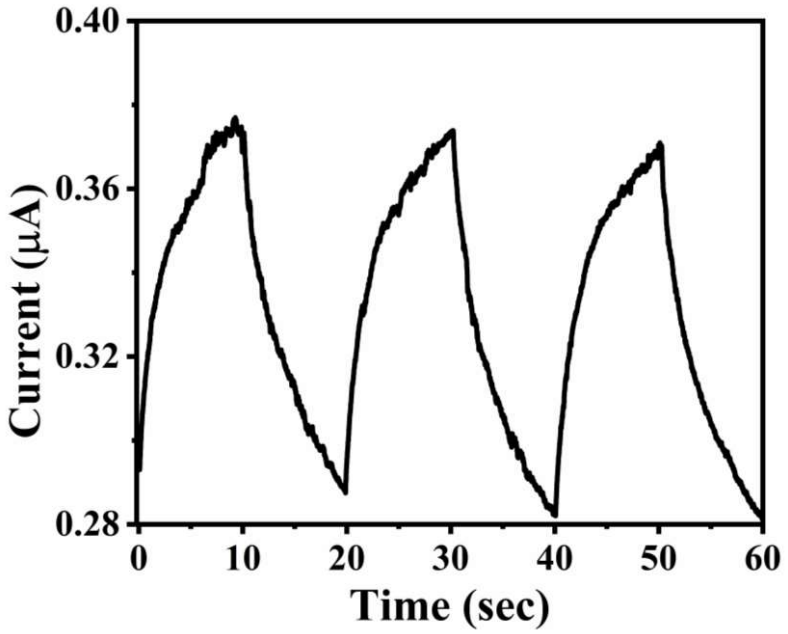

Figure 2.16: Transient response of the proposed heterojunction photodetector illuminated by the white pulse light (optical power density of ~40.3 μW/cm^2).

The characteristics reveal that the transient response of the photodetector is repeatable. The speed of the photodetector is measured in terms of rise time and fall time, which are calculated as time elapsed to change the current from 10% to 90% and 90% to 10%, respectively. The rise time and fall time characteristics of the photodetector are shown in Figure 2.17. It is found that the photodetector has rise time and fall time of 7.21 s and 6.23 s, respectively.

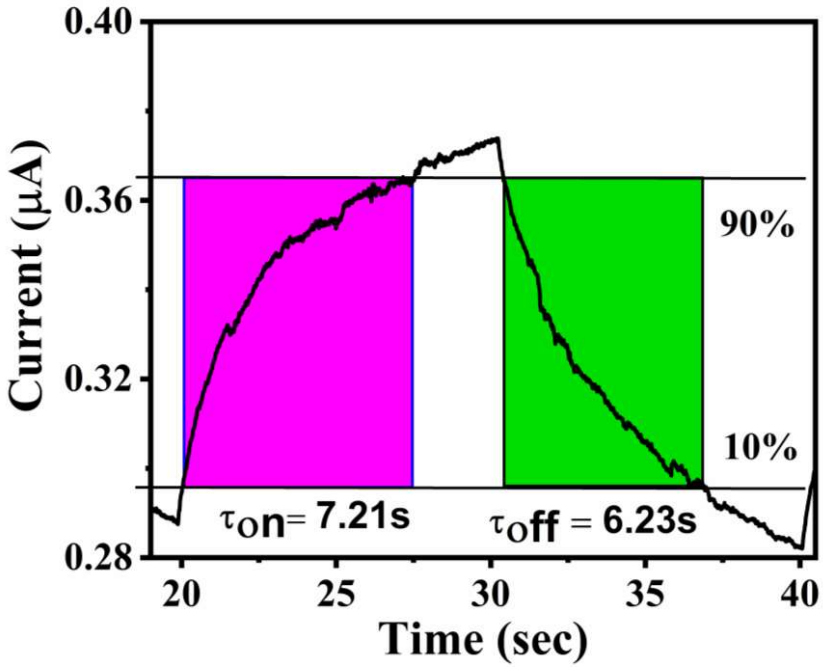

Figure 2.17: Single-cycle of the transient response for rise time and fall time calculation.

2.4 Conclusion

In this chapter, the fabrication and characterization of an ITO/ZnO NPs/BFO NPs/PEDOT: PSS/Ag heterojunction based white light photodetector has been demonstrated. ZnO NPs and BFO NPs are synthesized using the sol-gel method and solid-state route. Then the morphological, structural, and optical of as-grown ZnO NPs and $BiFeO_3$ NPs have been analysed by SEM images, XRD analysis, and UV-Vis spectrum, respectively. The ZnO NPs are shown to have a wurtzite hexagonal structure, whereas the BFO NPs have a high phase purity rhombohedral crystalline structure, estimated optical band gaps of ~2.0 eV and ~3.2 eV are found for $BiFeO_3$ thin film and ZnO nanoparticles. The BFO NPs and ZnO NPs act as the n-type active layer and an electron transport layer (ETL) in the fabricated photodetector device, respectively. The proposed photodetector exhibits a maximum responsivity of ~34 mA/W, and EQE of ~8.8% over the wavelength 450 to 650 nm with a rise time of 7.21 s and fall time of 6.23 s at the applied voltage of -2 V.